Population-based asymmetric margins for moving targets in real-time tumor tracking

（リアルタイム腫瘍追尾技術における動体標的に対する患者集団統計量に基づいた非対称マージン計算式の導出）

木藤　哲史

Population-based asymmetric margins for moving targets in real-time tumor tracking

Satoshi Kito[1,2] | Nobutaka Mukumoto[3] | Mitsuhiro Nakamura[1,3] |
Hiroaki Tanabe[4] | Katsuyuki Karasawa[2,†] | Masaki Kokubo[5] | Takashi Sakamoto[6] |
Yusuke Iizuka[3] | Michio Yoshimura[3] | Yukinori Matsuo[3] | Masahiro Hiraoka[7] |
Takashi Mizowaki[3]

[1]Department of Advanced Medical Physics, Graduate School of Medicine, Kyoto University, Sakyo-ku, Kyoto, Japan

[2]Division of Radiation Oncology, Department of Radiology, Tokyo Metropolitan Cancer and Infectious Diseases Center Komagome Hospital, Bunkyo-ku, Tokyo, Japan

[3]Department of Radiation Oncology and Image-Applied Therapy, Graduate School of Medicine, Kyoto University, Sakyo-ku, Kyoto, Japan

[4]Department of Radiological Technology, Kobe City Medical Center General Hospital, Kobe, Hyogo, Japan

[5]Department of Radiation Oncology, Kobe City Medical Center General Hospital, Kobe, Hyogo, Japan

[6]Department of Radiation Oncology, Kyoto-Katsura Hospital, Nishikyo-ku, Kyoto, Japan

[7]Department of Radiation Oncology, Japanese Red Cross Society Wakayama Medical Center, Wakayama, Japan

Correspondence
Mitsuhiro Nakamura, Department of Advanced Medical Physics, Graduate School of Medicine, Kyoto University, 53 Kawahara-cho, Shogoin, Sakyo-ku, Kyoto 606-8507, Japan.
Email: m_nkmr@kuhp.kyoto-u.ac.jp

Funding information
AMED, Grant/Award Number: JP17ck0106303

Abstract

Background: Both geometric and dosimetric components are commonly considered when determining the margin for planning target volume (PTV). As dose distribution is shaped by controlling beam aperture in peripheral dose prescription and dose-escalated simultaneously integrated boost techniques, adjusting the margin by incorporating the variable dosimetric component into the PTV margin is inappropriate; therefore, geometric components should be accurately estimated for margin calculations.

Purpose: We introduced an asymmetric margin-calculation theory using the guide to the expression of uncertainty in measurement (GUM) and intra-fractional motion. The margins in fiducial marker-based real-time tumor tracking (RTTT) for lung, liver, and pancreatic cancers were calculated and were then evaluated using Monte Carlo (MC) simulations.

Methods: A total of 74 705, 73 235, and 164 968 sets of intra- and inter-fractional positional data were analyzed for 48 lung, 48 liver, and 25 pancreatic cancer patients, respectively, in RTTT clinical trials. The 2.5th and 97.5th percentiles of the positional error were considered representative values of each fraction of the disease site. The population-based statistics of the probability distributions of these representative positional errors (PD-RPEs) were calculated in six directions. A margin covering 95% of the population was calculated using the proposed formula. The content rate in which the clinical target volume (CTV) was included in the PTV was calculated through MC simulations using the PD-RPEs.

Results: The margins required for RTTT were at most 6.2, 4.6, and 3.9 mm for lung, liver, and pancreatic cancer, respectively. MC simulations revealed that the median content rates using the proposed margins satisfied 95% for lung and liver cancers and 93% for pancreatic cancer, closer to the expected rates than the margins according to van Herk's formula.

Conclusions: Our proposed formula based on the GUM and motion probability distributions (MPD) accurately calculated the practical margin size for fiducial marker-based RTTT. This was verified through MC simulations.

KEYWORDS
asymmetric margin, GUM, motion probability distribution, multi-institutional study, real-time tumor tracking

1 | INTRODUCTION

In general, lung, liver, and pancreatic cancers are categorized as moving targets.[1] When treating such targets, inter- and intra-fraction variations must be addressed during treatment.[2–5] The former can be minimized via image guidance, for example, using cone-beam computed tomography or kV x-ray images.[3,6] Additionally, the effects the latter, for example, respiratory motion and changes in amplitude and baseline drift, can be mitigated via abdominal compression,[7,8] breath-holding,[9] respiratory gating,[2,5,10–15] and real-time tumor tracking (RTTT).[16–27]

Margin settings affect clinical outcomes, which are crucial for moving targets. Excessive margins include parts of organs at risk (OARs), causing radiation-induced toxicity, whereas an insufficient margin may result in a geometric miss, leading to local recurrence. Thus, each facility must estimate appropriate margins according to specific treatment techniques.

When determining the margin for the planning target volume (PTV), a combination of geometric and dosimetric components is commonly considered.[28] Most institutions determine geometric components based on previously acquired data. For the moving targets, motion probability distributions (MPD) are patient-specific and asymmetric,[29,30] which is a possible factor for appropriate margin sizes. In addition, Witte et al. found that the target size was another factor that causes changes in the minimum margin required for random geometric uncertainties.[31] Thus, these factors should be considered in PTV margin calculations. In contrast, various prescription strategies, such as the peripheral dose prescription and dose-escalated simultaneously integrated boost, have been recently used in clinical practice. The dosimetric component, which is incorporated into van Herk's formula,[28] is not constant in such strategies because the dose distribution is shaped by controlling the beam aperture; therefore, adjusting the margin by incorporating the variable dosimetric component into the PTV margin is inappropriate. Figure 1 illustrates an example where the incorporation of the dosimetric component into margin calculations is inappropriate, indicating that the penumbra width is dependent on respiratory phases in RTTT. Thus, an accurate estimation of geometric components considering MPD and target size is crucial for margin calculations.

Positional uncertainty can be categorized into inter- and intra-patient positional uncertainty. The latter can be the main component when MPD is observed. We believe that the guide to the expression of uncertainty in measurement (GUM), as recommended by regulatory bodies like the International Organization for Standardization and the *Bureau International des Poids et Mesures*, would be suitable for estimating geometric uncertainties.[32] However, because MPDs are not sym-metric as shown in Figure 2, it is challenging to simply combine inter- and intra-patient positional uncertainties using GUM. The tail of MPDs in each direction, which would contribute to the determination of margin size, varies around the patient population mean with patient population uncertainty, and it further varies with individual patient uncertainty. Assuming tail variations have gaussian distribution, the variations combined by GUM would be theoretically accurate.

Since 2015, we have been performing multi-institutional phase II studies on fiducial marker-based RTTT in lung, liver, and pancreatic cancer patients with three-dimensional (3D) respiratory motions of >10 mm using a gimbaled x-ray head.[33–35] Thus, we obtained a substantial number of inter- and intra-fraction target positions, which could be utilized to determine the margin size. The purpose of this study was two-fold. We introduced an asymmetric margin-calculation theory based on the combination of GUM and MPDs and estimated the margins in fiducial marker-based RTTT with a gimbaled x-ray head for lung, liver, and pancreatic cancers. Further, the obtained results were verified through Monte Carlo (MC) simulations.

2 | MATERIALS AND METHODS

2.1 | Summary of the clinical study

A total of 121 patients, comprising 48 lung, 48 liver, and 25 pancreatic cancer patients, were enrolled from four domestic institutions for the study. This clinical study was approved by the Institutional Ethics Review Board. Informed consent was obtained from all patients, and the trials were registered in the UMIN Clinical Trials Registry.[33–35] Information on the registered cases is summarized in Table 1.

Two or more spherical gold markers (Disposable Gold Marker, FMR-201CR; Olympus Medical Systems, Tokyo, Japan) were implanted around the lung tumor using a bronchoscope, whereas a cylindrical gold marker (Visicoil; IBA, Louvain-la-neuve, Belgium) was inserted within or close to the tumor percutaneously or endoscopically for liver and pancreatic cancer patients. The 3D respiratory motion of the tumor indicated by the fiducial markers exceeded 10 mm, according to fluoroscopy or four-dimensional computed tomography results obtained from the simulation.

2.2 | Gimbaled tracking procedure

After initial translational and rotational setup errors were corrected based on bone anatomy, a correlation model was constructed between the target position indicated by the fiducial marker (detected target position) and the
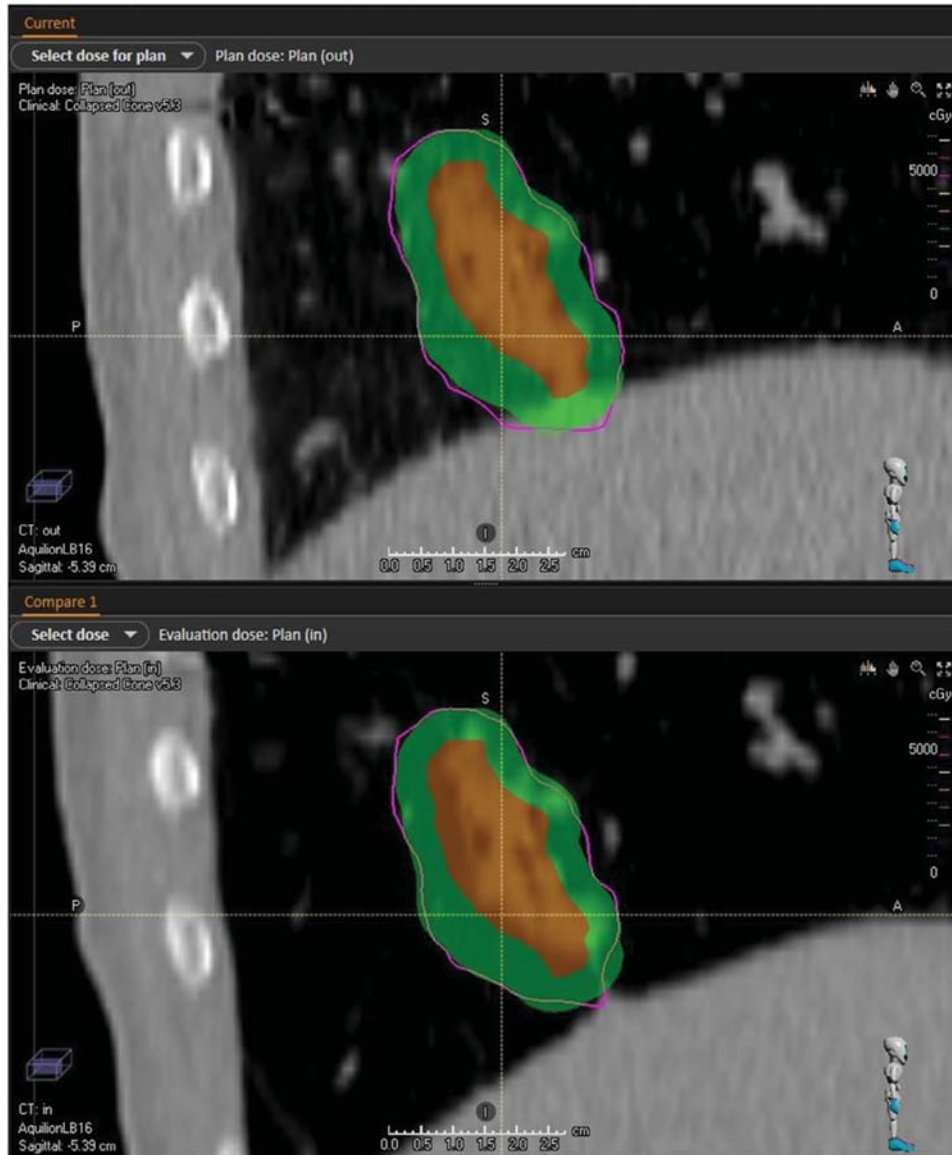
FIGURE 1 Example of the dose perturbation near the diaphragm. The upper part shows the planning dose distribution in the exhale CT, and the lower part shows the evaluation dose distribution in the inhale CT in real-time tumor tracking. Clinical target volume (solid red), planning target volume with a 5-mm margin (solid green), and the prescribed isodose line (solid magenta) are shown in the figures.

infrared reflective (IR) marker positions on the abdominal wall. The fiducial marker positions were monitored for 20−40 s using an orthogonal kV x-ray imaging subsystem while monitoring the IR marker motion.[20]

During beam delivery, the predicted target position was calculated from the correlation model, and the position of the fiducial markers was monitored using the orthogonal kV x-ray imaging subsystem every second through the console display to ascertain accurate irradiation. During beam delivery, the predicted and detected target positions were obtained in chronological order and in the left–right (L–R), anterior–posterior (A–P), and superior–inferior (S–I) directions. The mechanical isocenter is the origin of the coordinates. Further details

on the gimbaled tracking procedure are available in literature.[18,20,25,36]

2.3 | Proposed margin calculation method

We calculated the margins using the population-based mean difference (Y), inter-patient uncertainty (υ), and intra-patient uncertainty (τ) of the population of a representative positional error (RPE) in each direction. RPE is defined later. Y defines the population-based mean of the differences between the daily treatment and mean positions of all fractions in each patient, υ is their
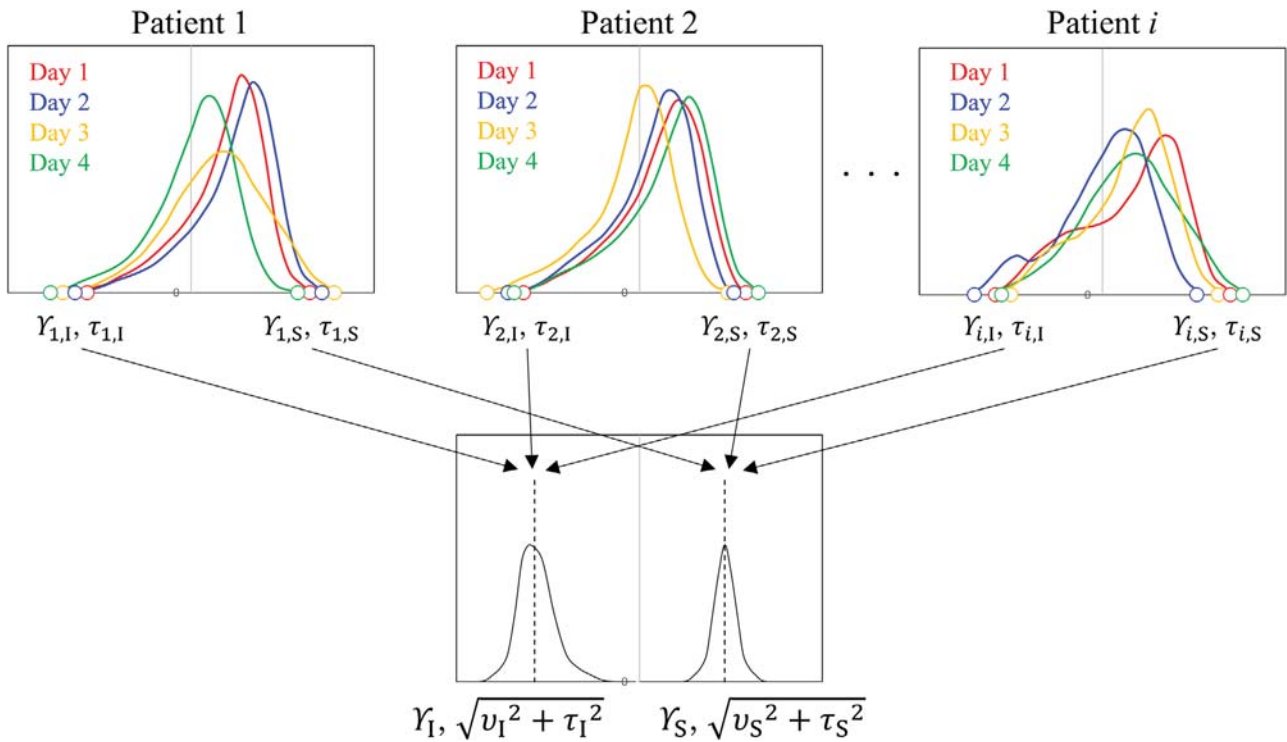
FIGURE 2 Scheme of calculating the asymmetric margin from the patient positioning error histogram. Y_i represents the population-based mean of the differences between the daily treatment and mean positions of all fractions, and τ_i represents the root-mean-square of the standard deviation (SD) of individual patient displacements for the ith patient. υ represents their population-based SD. Subscript I and S indicate the inferior and superior directions, respectively.

TABLE 1 Registered cases.

	Prescribed dose at PTV $D_{95\%}$	Delivery technique	Number of completions/ Accruing number	Number of analyses	Equivalent size of CTV[c] [mm]	Range of motion during beam delivery[c] [mm]
Lung[33]	50 Gy/4 fr.	Non-IMRT (multiple non-coplanar static beams)	47/48[a]	187[b]	Sphere diameter 16.9 (8.0−28.3)	13.7 (4.5−28.1)
Liver[34]	40 Gy/5 fr.	Non-IMRT (multiple non-coplanar static beams)	48/48	235[b]	Sphere diameter 14.5 (8.7−27.8)	11.7 (4.3−40.9)
Pancreas[35]	48 Gy/15 fr.	Fixed gantry SIB-IMRT	25/25	375	Cubic length 47.8 (39.6−65.1)	9.7 (3.5−25.3)

Abbreviations: CTV, clinical target volume; fr., fractions; IMRT, intensity-modulated radiotherapy; PTV $D_{95\%}$, dose covering 95% of the planning target volume; SIB, simultaneous integrated boost.

[a]One patient was not treated with RTTT because the abdominal-wall motion was not well correlated with tumor movement.

[b]The fiducial markers were not detected due to an in-house software issue in one and five fractions for a lung and liver cancer patient, respectively.

[c]Data are presented as the median (minimum–maximum).

population-based standard deviation (SD), and τ is the root-mean-square of the SD of individual patient displacements. Here, υ and τ, assumed to have an equal contribution, are combined according to the GUM,[32] and the margin theory is expressed as

$$Margin = Y + k \cdot \sqrt{\upsilon^2 + \tau^2}, \qquad (1)$$

where k represents the coverage factor of $\sqrt{\upsilon^2 + \tau^2}$ used to satisfy the required probability. The margin covering 95% of the population was calculated using the proposed formula. The optimal k varies depending on the shape and size of the CTV. Furthermore, k can be determined fairly precisely when the CTV has a spherical or cubic shape.

2.4 | Spherical target

In a spherical extended volume (EXV) with a clinical target volume (CTV) radius extended by Y, it is assumed that arbitrary points on the EXV surface vary with the SD $\varepsilon = \sqrt{v^2 + \tau^2}$ according to a 3D Gaussian distribution in each direction. Here, $f = k\varepsilon$ is the expansion width for any arbitrary point on the EXV surface to be included in the PTV with the required probability. Figure 3a presents an overview of the calculation geometry, where $w(r_{CTV}, f, \theta)$ is the distance between point Q located at the top of the EXV and PTV considering elevation angle θ.

$$w(r_{CTV}, f, \theta) = \sqrt{r_{PTV}^2 - \cos^2\theta \cdot r_{EXV}^2} - \sin\theta \cdot r_{EXV},$$

$$(2)$$

where r_{CTV}, $r_{EXV} = r_{CTV} + Y$, and $r_{PTV} = r_{EXV} + f$ are the radii of the CTV, EXV, and PTV, respectively. Next, when point p varies in a 3D Gaussian distribution with the same SD ε in each direction around Q, the probability that p exists within radius $w(r_{CTV}, f, \theta)$ is

$$g(w(r_{CTV}, f, \theta)) = \frac{-\sqrt{2} \cdot w(r_{CTV}, f, \theta)}{\sqrt{\pi} \cdot \varepsilon} \cdot e^{-\frac{w(r_{CTV}, f, \theta)^2}{2 \cdot \varepsilon^2}}$$
$$+ \operatorname{erf}\left(\frac{w(r_{CTV}, f, \theta)}{\sqrt{2} \cdot \varepsilon}\right).$$

$$(3)$$

Subsequently, the ratio $s(\theta)$ of the area from θ to $\theta + d\theta$ to the total area of the sphere centered at Q is given as

$$s(\theta) = \frac{1}{2} \cdot \cos\theta \cdot d\theta.$$

$$(4)$$

Therefore, content probability $p(\theta)$ that p exists within radius $w(r_{CTV}, f, \theta)$ in θ to $\theta + d\theta$ is

$$p(\theta) = g(w(r_{CTV}, f, \theta)) \cdot s(\theta)$$
$$= \frac{1}{2} \cdot g(w(r_{CTV}, f, \theta)) \cdot \cos\theta \cdot d\theta.$$

$$(5)$$

Finally, the total content probability $P(r_{CTV}, f)$ for the entire sphere is calculated by integrating Equation (5) with θ as

$$P(r_{CTV}, f) = \frac{1}{2} \cdot \int_{-\frac{\pi}{2}}^{\frac{\pi}{2}} \left\{ \frac{-\sqrt{2} \cdot w(r_{CTV}, f, \theta)}{\sqrt{\pi} \cdot \varepsilon} \cdot e^{-\frac{w(r_{CTV}, f, \theta)^2}{2 \cdot \varepsilon^2}} \right.$$
$$\left. + \operatorname{erf}\left(\frac{w(r_{CTV}, f, \theta)}{\sqrt{2} \cdot \varepsilon}\right) \right\} \cdot \cos\theta \cdot d\theta. \quad (6)$$
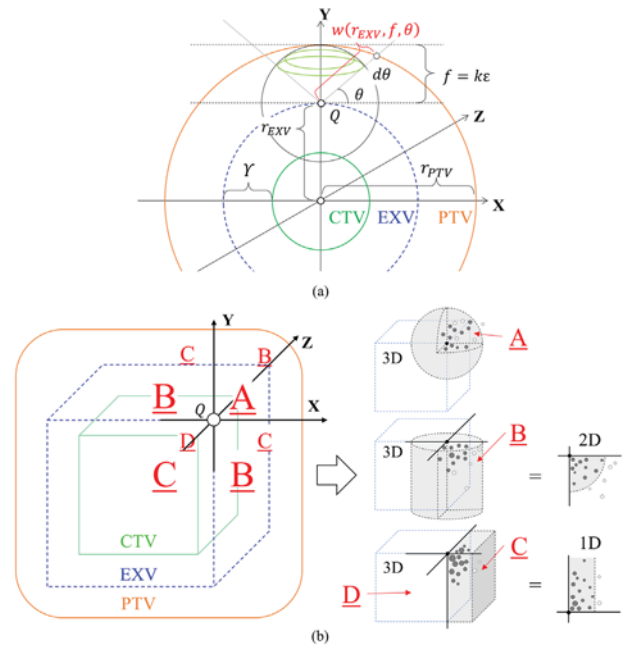

FIGURE 3 Diagram for theoretically calculating the margin between the clinical target volume (CTV) and planning target volume (PTV): (a) extended volume (EXV) is the volume obtained by expanding the radius from the CTV by Y. (b) If the CTV is a cube, the EXV and PTV are generated according to the same rules as those for a sphere.

By specifying $P(r_{CTV}, f)$ and r_{CTV} in Equation (6), f and k are obtained.

Figure 4 shows the relationship between k and $P(r_{CTV}, f)$ at a certain r_{EXV} relative to ε. With $r_{EXV} = 0\varepsilon$, $P(r_{CTV}, f)$ is the same content probability as van Herk's formula. In this study, $r_{EXV} = 2\varepsilon$ can be applied to CTVs with radii greater than 1 mm. The minimum CTV radius for the lung and liver cases was 4 mm (Table 1), and the calculated r_{EXV} was considerably larger than twice ε in each direction. Subsequently, a margin that satisfies $P(r_{CTV}, f) = 95\%$ or higher was expected in this study. Therefore, by determining $k = 2.0$, as shown in Figure 4 at $r_{EXV} = 2\varepsilon$ and $P(r_{CTV}, f) = 95\%$, this value was applied to calculate the margins in the lung and liver cancer cases. In the case of $k = 2.0$ at $r_{EXV} = 3\varepsilon$ or higher, $P(r_{CTV}, f) \geq 96\%$ is obtained.

2.5 | Cubic target

The gross tumor volume (GTV) included the tumor and metastatic lymph nodes. The CTV was defined as GTV plus a 5-mm margin as well as the retropancreatic space and the paraaortic lymph nodes between the celiac axis and superior mesenteric artery.[26] As the determination of the CTV in pancreatic cancer is different from that in lung and liver cancer, a cubic CTV shape was considered as an example of a well-defined shape to calculate the
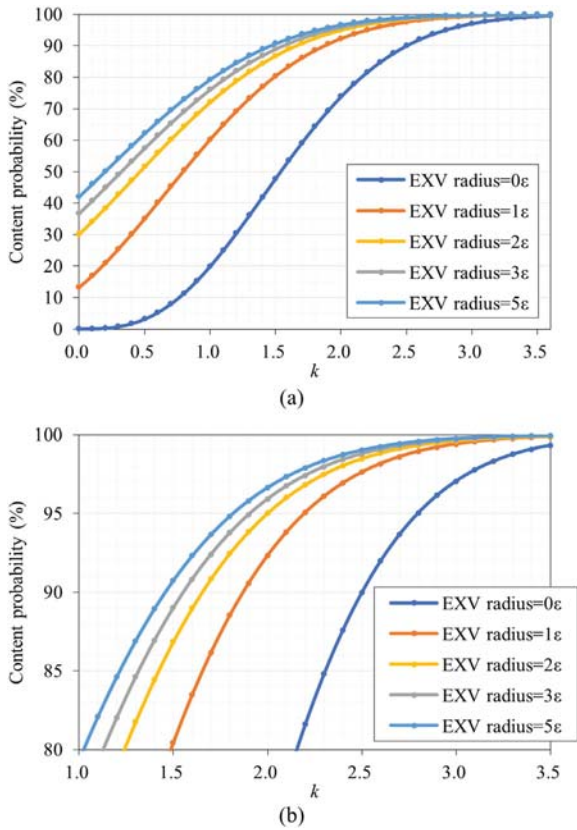
FIGURE 4 (a) Relationship between coefficient k and content probability for the tumor radii of $0\varepsilon, 1\varepsilon, 2\varepsilon, 3\varepsilon$, and 5ε. (b) Enlarged area of interest. $\varepsilon = \sqrt{v^2 + \tau^2}$ is the combined uncertainty, where v and τ represent the inter- and intra-patient uncertainties, respectively.

margin for pancreatic cancer. However, the side length of the cube was assumed to be sufficiently greater than ε. We consider a case where point p varies in a 3D Gaussian distribution centered at a certain vertex Q in an EXV extended by Y from the CTV. Furthermore, the PTV is defined as the volume expanded by $f = k\varepsilon$ from the EXV. As shown in the geometry in Figure 3b, the PTV is first divided into eight spaces centered at Q. In octant $\underline{A}$, the probability that p is included in the PTV is $P_{3D}(f) = \frac{-\sqrt{2} \cdot f}{\sqrt{\pi} \cdot \varepsilon} \cdot e^{-\frac{f^2}{2 \cdot \varepsilon^2}} + \text{erf}(\frac{f}{\sqrt{2} \cdot \varepsilon})$, based on a 3D Gaussian distribution. In octant $\underline{B}$, since this area is a fan-shaped cylinder, the height parameter can be omitted from the probability calculation. Therefore, it can be strictly computed using a 2D Gaussian instead of 3D. The probability is $P_{2D}(f) = 1 - \exp(-\frac{f^2}{2 \cdot \varepsilon^2})$. In octant $\underline{C}$, the probability is further simplified as $P_{1D}(f) = \text{erf}(\frac{f}{\sqrt{2} \cdot \varepsilon})$, based on a 1D Gaussian distribution. In octant $\underline{D}$, which is within the EXV, the probability is unity. Accordingly, the total probability $P(f)$ for the entire region is calculated as

$$P(f) = \frac{1 \cdot P_{3D}(f) + 3 \cdot P_{2D}(f) + 3 \cdot P_{1D}(f) + 1 \cdot 1}{8}. \quad (7)$$

For $P(f) = 95\%$, the numerical calculation using Equation (7) satisfies $f = k \cdot \varepsilon = 2.33\varepsilon$.

2.6 | Sampling of the 2.5th and 97.5th percentiles of the tracking error probability distribution and verification

The 2.5th (corresponding to the L, I, and P directions) and 97.5th (corresponding to the R, S, and A directions) percentiles of the positional error histogram in each fraction for each patient were considered as the RPE values. In non-respiratory motion management (non-RM), RPE was defined as the difference between the radiation isocenter and detected target positions. In RTTT, it is the difference between the predicted and detected target positions. Y, v, and τ in Equation (1) in each direction for the lung, liver, and pancreatic cancers were calculated from each PD-RPE.

As Equation (1) is derived based on the assumption that the PD-RPE follows a normal distribution, a theoretical error occurs when the PD-RPE deviates from the normal distribution. Therefore, the goodness of fit of the PD-RPE with the normal distribution, in each direction, was confirmed using the Kolmogorov−Smirnov test.

2.7 | Verification of the theoretical margin formula using MC simulations

MC simulations were performed using a simple geometry and the actual PD-RPE at each site for evaluating the validity of the margin when the PD-RPE cannot be regarded as a normal distribution. Whether any point $p(x, y, z)$ in the CTV, which moves in six directions, deviates from the PTV is a stochastic process. The content rate in which p is included in the PTV is given by

$$\text{Content rate} = \frac{\textit{Number of trials included in the PTV}}{\textit{Total number of trials}},$$

$$(8)$$

where p was sampled according to the PD-RPEs. The total number of trials was set to 10 000 such that the statistical error was less than 0.1% in each situation.

As an example of a simplified CTV shape, a spherical shape with diameter r was assumed for the lung and liver tumors. The equivalent diameter was selected from the median CTV volume collected in the clinical study. The lung and liver diameters were set to 16.9 and 14.5 mm, respectively (Table 1). Conversely, a cubic shape with side-length $l = 47.8$ mm was assumed for pancreatic cancer (Table 1). The PTV was generated according to Equation (2) with coefficient k (2.0 for lung and liver cancers, 2.33 for pancreatic cancer) from the CTV. For the spherical shape, any point on the CTV surface can deviate from the PTV with the highest probability.
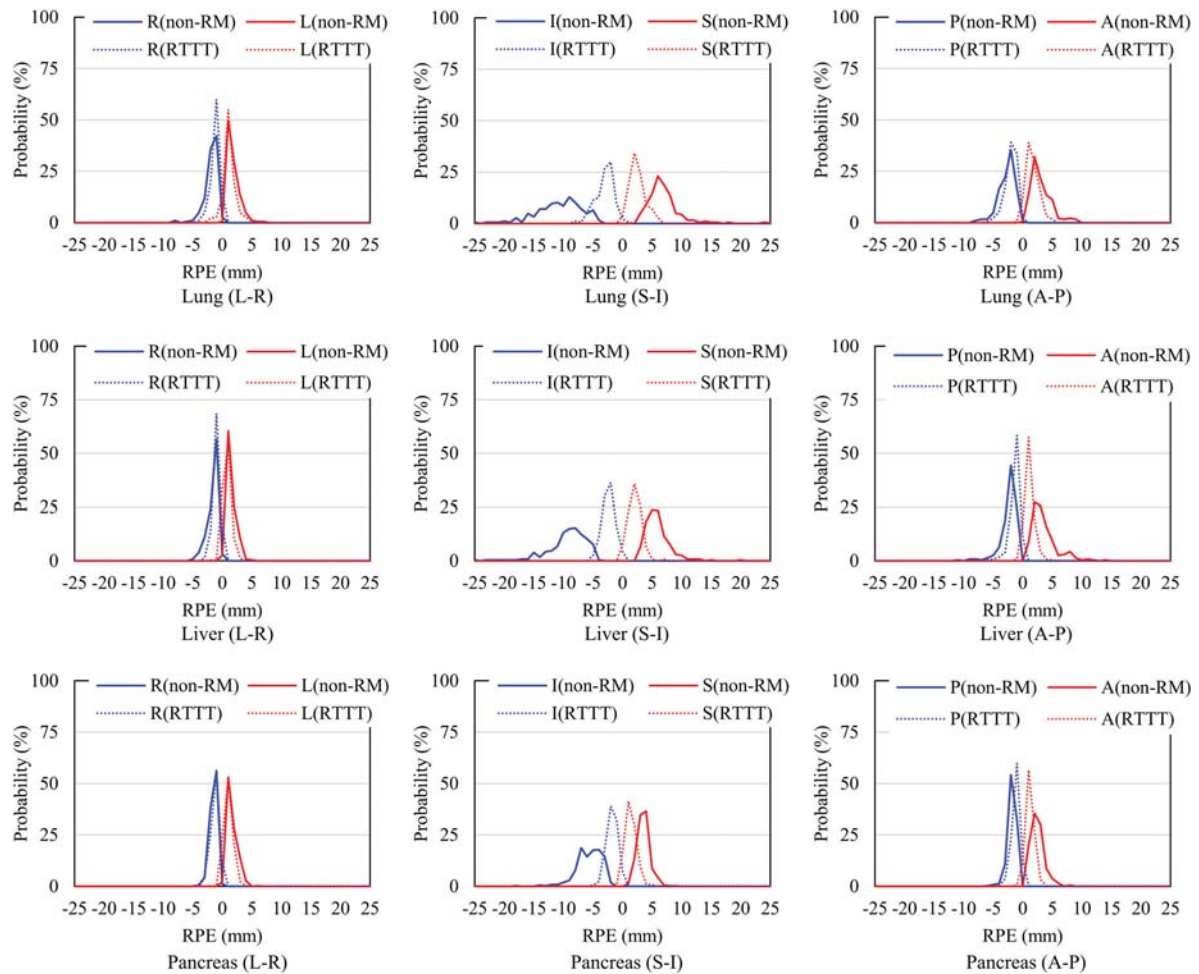
FIGURE 5 Probability distributions of representative positional errors (PD-RPEs) in the left (L), right (R), superior (S), inferior (I), anterior (A), and posterior (P) directions for non-respiratory management (solid) and real-time tracking (dotted) for lung, liver, and pancreatic cancers.

Coordinates on the axes and surface in the left (L), right (R), superior (S), inferior (I), anterior (A), and posterior (P) directions were selected as evaluation points. For the cubic shape, as the eight vertices have the highest probability of deviating from the PTV, their coordinates were selected as the evaluation points. The coordinates at the designated evaluation points on the CTV were sampled based on the PD-RPE using uniform random numbers. Finally, it was determined whether the coordinates of each evaluation point on the CTV were included in the PTV, and the content rate was obtained.

To evaluate the statistical significance of the content rates between our formula and van Herk's equation, a Wilcoxon signed-rank test was performed.[28] The level of significance was set to 0.05, and all statistical analyses were performed using MATLAB (version R2019a).

3 | RESULTS

In total, 120 patients were successfully treated with RTTT. One lung cancer patient was not treated with RTTT because the abdominal-wall motion was not well-correlated with tumor movement. In addition, the fiducial markers were not detected due to an in-house software issue in one and five fractions for individual lung and liver cancer patients, respectively. Consequently, 74 705, 73 235, and 164 968 sets of inter- and intra-fractional positional data were analyzed for the lung, liver, and pancreatic cancer patients, respectively, during the overall treatment.

The PD-RPEs for the lung, liver, and pancreas in each direction are shown in Figure 5. Compared to the PD-RPEs in non-RM cases, those in the RM cases distributed around an RPE of 0 mm. Table 2 summarizes the results of the p-values of the goodness of the PD-RPE of RTTT for the lung, liver, and pancreas with the normal distribution using the Kolmogorov−Smirnov test.

Table 3 summarizes the statistical values for calculating the margins for non-RM and RTTT. Although there were some exceptions, the statistical values for RTTT were smaller than those for non-RM. Among the three metrics, Y had the largest impact on margin size. The margin sizes were asymmetric for each axis.

TABLE 2 *p*-values of the goodness of the probability distribution of representative positional errors of real-time tumor tracking for the lung, liver, and pancreas with the normal distribution using the Kolmogorov–Smirnov test.

	L	R	S	I	A	P
Lung	0.034*	0.051	0.233	0.267	0.092	0.042*
Liver	0.088	0.027*	0.629	0.285	0.030*	0.061
Pancreas	0.099	0.018*	0.096	0.018*	0.010*	0.029*

Abbreviations: A, anterior; I, inferior; L, left; P, posterior; R, right; S, superior.
*The asterisk indicates that the *p*-value exceeds the 5% significance level using the Wilcoxon signed-rank test.

For non-RM, the margins were at most 18.9, 16.4, and 10.8 mm for lung, liver, and pancreatic cancer, respectively. The margin, especially in the inferior direction, was large. In contrast, those were at most 6.2, 4.6, and 3.9 mm, respectively, for RTTT. The margins in the A–P axis were the second largest, followed by those in the L–R axis.

Table 4 lists the results of the MC simulations for the margin. The median content rates of the designated evaluation points were 95% or more for lung and liver cancer and 93% for pancreatic cancer, using our formula. In contrast, those according to van Herk's equation were 89% for pancreatic cancer and more than 97% for lung and liver cancer, which was higher than their expectation. There were significant differences in the content rates for lung and pancreatic cancer ($p < 0.05$).

TABLE 4 Probabilities of the numbers of each point (the farthest end points on the left, right, anterior, posterior, superior, and inferior on the spherical clinical target volume (CTV), and the eight vertices on the cubic CTV) included in the planning target volume when the margins calculated using van Herk's equation and the proposed equation in this study are added to the CTV in the Monte Carlo simulation.

Site	Shape	This study[a] [%]	van Herk[a] [%]	*p*-value
Lung	Sphere	96.0 (95.1–96.7)	98.0 (96.5–98.5)	<0.05[b]
Liver	Sphere	96.7 (95.8–98.4)	97.6 (96.7–98.6)	0.193
Pancreas	Cube	93.2 (92.6–93.9)	88.8 (87.1–90.6)	<0.05[b]

[a]Data are shown as the median (minimum–maximum).
[b]This indicates that the *p*-value exceeds the 5% significance level using the Wilcoxon signed-rank test.

4 | DISCUSSION

Several researchers have reported the margin for RTTT with CyberKnife (CK).[22,27] Descovich et al. calculated the symmetric margin in CK treatments using fiducial markers of 4.4, 6.8, and 4.7 mm in the L–R, S–I, and A–P directions, respectively.[22] Yang et al. reported total tracking errors of less than 4 mm in the X-sight lung tracking.[27] These results are slightly different from ours, which can be attributed to following reasons: (i) larger tumor motion and more patients in our study, (ii) asymmetric margin calculation concept with the 2.5th and 97.5th percentiles of the PD-RPEs in each direction, and (iii) unlike van Herk's theory intending to cover

TABLE 3 Margins between the clinical target volume and planning target volume for the lung, liver, and pancreatic cancers.

		Non-respiratory motion management						Real-time tumor tracking					
		L	R	S	I	A	P	L	R	S	I	A	P
Lung	Y [mm]	1.8	1.9	6.9	10.8	3.1	2.8	1.1	1.1	2.5	3.0	1.6	2.0
	υ [mm]	1.0	1.1	2.3	3.6	1.6	1.3	0.9	0.6	1.0	1.3	0.9	0.8
	τ [mm]	0.5	0.5	1.7	1.9	1.0	0.7	0.6	0.5	1.0	0.9	0.8	0.7
	Margin (proposed) [mm]	4.0	4.3	12.6	18.9	6.8	5.7	3.2	2.7	5.3	6.2	3.9	4.2
	Margin (van Herk)※ [mm]	4.6	4.9	13.8	21.0	7.7	6.5	3.8	3.0	5.7	6.9	4.2	4.6
Liver	Y [mm]	1.4	1.5	5.9	9.4	3.6	2.4	0.8	1.0	2.1	2.4	1.1	1.3
	υ [mm]	0.7	0.9	1.9	3.0	2.0	1.3	0.5	0.4	0.8	0.7	0.6	0.7
	τ [mm]	0.5	0.4	1.3	1.9	1.0	0.8	0.4	0.4	0.8	0.9	0.5	0.5
	Margin (proposed) [mm]	3.1	3.4	10.5	16.4	8.0	5.3	2.1	2.1	4.3	4.6	2.7	3.1
	Margin (van Herk)※ [mm]	3.5	4.0	11.5	18.2	9.3	6.1	2.3	2.2	4.6	4.7	3.1	3.5
Pancreas	Y [mm]	1.6	1.5	3.5	5.6	2.5	1.9	1.0	1.2	1.4	1.8	1.2	1.2
	υ [mm]	0.7	0.5	0.8	1.9	1.1	0.5	0.3	0.4	0.5	0.6	0.4	0.4
	τ [mm]	0.5	0.4	0.7	1.1	0.5	0.5	0.6	0.6	0.8	0.7	0.6	0.5
	Margin (proposed) [mm]	3.6	2.8	6.1	10.8	5.2	3.5	2.6	2.9	3.6	3.9	2.9	2.7
	Margin (van Herk)※ [mm]	3.7	2.9	6.2	11.2	5.4	3.6	2.3	2.8	3.2	3.7	2.7	2.6

Abbreviations: A, anterior; I, inferior; L, left; P, posterior; R, right; S, superior; Y, population-based mean of each patient's mean value; τ, root mean square of each patient's standard deviation; υ, population-based standard deviation of each patient's mean value.
※For reference only, each component in each direction was applied to simplified van Herk's formula ($Y + 2.5\upsilon + 0.7\tau$).

90% of the population, the margin was intended to cover 95%. Generally, the accuracy of margin calculation depends on the number of patients. Although our proposed margins were based on a relatively small number of patients, the MC results indicated that the margins were acceptable for the expected probabilities.

There are few reports that have verified whether the calculated margin was valid using another method (for example, as in the MC simulation performed in this study).[37–39] Herschtal et al. performed MC simulations to validate the margin in a hypofractionated radiotherapy setting.[39] In other studies on RTTT, van Herk's equation was used without confirming the normality of the probability distributions of the various error components.[23,27] Although the PD-RPEs were obtained from a substantial number of 3D tracking errors in this study, there were certain sites and directions in which the normality of the probability distribution could not be proved, which differed from the premise of the proposed equation. Nevertheless, the MC simulation based on the PD-RPE yielded expected results. However, the median content rate for pancreatic cancer obtained using our equation was 93%, which was slightly insufficient as margins (Table 4). This may be because the PD-RPE in the worst direction was not normally distributed. In contrast, content rates based on van Herk's equation were more than 97% for lung and liver cancers. When σ is less than 3.2 mm in a medium, the margin based on the simplified expression in van Herk's theory is larger than the exact margin (approximately 0.5-mm overestimation for $\sigma = 1$ mm), as described in Ref..[28] However, the subtraction of the component causing the overestimation from the calculated margin based on the simplified expression leads to insufficient margins for pancreatic cancer in this study. Therefore, van Herk's equation would provide insufficient margin sizes in RTTT. Overall, our proposed margin formula is appropriate for fiducial marker-based RTTT.

Despite its many advantages, there are several limitations to our approach. First, we did not fully consider the change in the geometric relationship between the tumor and the surrounding fiducial markers during respiration. Ueki et al. proposed 2.5 mm to ensure this uncertainty[4]; however, simply adding this value to our calculated margin would be excessive. When the respiratory phase images were registered based on the marker centroid, the resultant target volume was expected to compensate for the uncertainty in the positional relationship between the tumor and fiducial markers during respiration. Second, the predicted target positions were calculated based on the correlation model implemented in Vero4DRT. Poels et al. reported that the prediction accuracy of CK was similar to that of Vero4DRT[40]; therefore, the derived margin size is applicable to CK tracking. Third, when the gimbaled x-ray head tracked the predicted target position, mechanical errors occurred, which were not considered in this study; however, Mukumoto et al. revealed that prediction errors were the primary cause of tracking errors and that the mechanical errors were negligible.[17,20]

5 | CONCLUSION

Based on a combination of the GUM and the MPD of the tracking errors, we proposed a theoretically determined margin-calculation formula for RTTT. Margins were derived with the proposed formula using the PD-RPE based on the actual tracking errors for lung, liver, and pancreatic cancers. These margins were verified through MC simulations, and the expected content rate was achieved with high reliability for all sites. Therefore, the proposed formula appropriately calculated the practical margin size for the fiducial marker-based RTTT.

DATA AVAILABILITY STATEMENT
The data that support the findings of this study are not available.

REFERENCES

1. Keall PJ, Mageras GS, Balter JM, et al. The management of respiratory motion in radiation oncology report of AAPM Task Group 76. *Med Phys*. 2006;33:3874-3900.
2. Shirato H, Suzuki K, Sharp GC, et al. Speed and amplitude of lung tumor motion precisely detected in four-dimensional setup and in real-time tumor-tracking radiotherapy. *Int J Radiat Oncol Biol Phys*. 2006;64:1229-1236.
3. Sonke JJ, Rossi M, Wolthaus J, van Herk M, Damen E, Belderbos J. Frameless stereotactic body radiotherapy for lung cancer using four-dimensional cone beam CT guidance. *Int J Radiat Oncol Biol Phys*. 2009;74:567-574.
4. Ueki N, Matsuo Y, Nakamura M, et al. Intra- and interfractional variations in geometric arrangement between lung tumours and implanted markers. *Radiother Oncol*. 2014;110:523-528.
5. Shiinoki T, Hanazawa H, Yuasa Y, Fujimoto K, Uehara T, Shibuya K. Verification of respiratory-gated radiotherapy with new real-time tumour-tracking radiotherapy system using cine EPID images and a log file. *Phys Med Biol*. 2017;62:1585-1599.
6. Sonke JJ, Lebesque J, van Herk M. Variability of four-dimensional computed tomography patient models. *Int J Radiat Oncol Biol Phys*. 2008;70:590-598.

7. Bouilhol G, Ayadi M, Rit S, et al. Is abdominal compression useful in lung stereotactic body radiation therapy? A 4DCT and dosimetric lobe-dependent study. *Phys Med*. 2013;29:333-340.

8. Mampuya WA, Nakamura M, Matsuo Y, et al. Interfraction variation in lung tumor position with abdominal compression during stereotactic body radiotherapy. *Med Phys*. 2013;40.

9. Boda-Heggemann J, Knopf AC, Simeonova-Chergou A, et al. Deep inspiration breath hold-based radiation therapy: a clinical review. *Int J Radiat Oncol Biol Phys*. 2016;94:478-492.

10. Wagman R, Yorke E, Ford E, et al. Respiratory gating for liver tumors: use in dose escalation. *Int J Radiat Oncol Biol Phys*. 2003;55:659-668.

11. Korreman SS, Juhler-Nøttrup T, Boyer AL. Respiratory gated beam delivery cannot facilitate margin reduction, unless combined with respiratory correlated image guidance. *Radiother Oncol*. 2008;86:61-68.

12. Giraud P, Morvan E, Claude L, et al. Respiratory gating techniques for optimization of lung cancer radiotherapy. *J Thorac Oncol*. 2011;6:2058-2068.

13. Shiinoki T, Kawamura S, Uehara T, et al. Evaluation of a combined respiratory-gating system comprising the TrueBeam linear accelerator and a new real-time tumor-tracking radiotherapy system: a preliminary study. *J Appl Clin Med Phys*. 2016;17:202-213.

14. Ehrbar S, Jöhl A, Tartas A, et al. ITV, mid-ventilation, gating or couch tracking – A comparison of respiratory motion-management techniques based on 4D dose calculations. *Radiother Oncol*. 2017;124:80-88.

15. Oh SA, Yea JW, Kim SK, Park JW. Optimal gating window for respiratory-gated radiotherapy with real-time position management and respiration guiding system for liver cancer treatment. *Sci Rep*. 2019;9:4384.

16. Keall PJ, Cattell H, Pokhrel D, et al. Geometric accuracy of a real-time target tracking system with dynamic multileaf collimator tracking system. *Int J Radiat Oncol Biol Phys*. 2006;65:1579-1584.

17. Mukumoto N, Nakamura M, Sawada A, et al. Positional accuracy of novel x-ray-image-based dynamic tumor-tracking irradiation using a gimbaled MV x-ray head of a Vero4DRT (MHI-TM2000). *Med Phys*. 2012;39:6287-6296.

18. Akimoto M, Nakamura M, Mukumoto N, et al. Predictive uncertainty in infrared marker-based dynamic tumor tracking with Vero4DRT. *Med Phys*. 2013;40:091705.

19. Mukumoto N, Nakamura M, Sawada A, et al. Accuracy verification of infrared marker-based dynamic tumor-tracking irradiation using the gimbaled x-ray head of the Vero4DRT (MHI-TM2000). *Med Phys*. 2013;40.

20. Mukumoto N, Nakamura M, Yamada M, et al. Intrafractional tracking accuracy in infrared marker-based hybrid dynamic tumour-tracking irradiation with a gimballed linac. *Radiother Oncol*. 2014;111:301-305.

21. Matsuo Y, Ueki N, Takayama K, et al. Evaluation of dynamic tumour tracking radiotherapy with real-time monitoring for lung tumours using a gimbal mounted linac. *Radiother Oncol*. 2014;112:360-364.

22. Descovich M, McGuinness C, Kannarunimit D, et al. Comparison between target margins derived from 4DCT scans and real-time tumor motion tracking: insights from lung tumor patients treated with robotic radiosurgery. *Med Phys*. 2015;42:1280-1287.

23. Iizuka Y, Matsuo Y, Ishihara Y, et al. Dynamic tumor-tracking radiotherapy with real-time monitoring for liver tumors using a gimbal mounted linac. *Radiother Oncol*. 2015;117:496-500.

24. Matsuo Y, Verellen D, Poels K, et al. A multi-centre analysis of treatment procedures and error components in dynamic tumour tracking radiotherapy. *Radiother Oncol*. 2015;115:412-418.

25. Mukumoto N, Nakamura M, Akimoto M, et al. Impact of sampling interval in training data acquisition on intrafractional predictive accuracy of indirect dynamic tumor-tracking radiotherapy. *Med Phys*. 2017;44:3899-3908.

26. Nakamura A, Hiraoka M, Itasaka S, et al. Evaluation of dynamic tumor-tracking intensity-modulated radiotherapy for locally advanced pancreatic cancer. *Sci Rep*. 2018;8:17096.

27. Yang ZY, Chang Y, Liu HY, Liu G, Li Q. Target margin design for real-time lung tumor tracking stereotactic body radiation therapy using CyberKnife Xsight Lung Tracking System. *Sci Rep*. 2017;7:10826.

28. van Herk M, Remeijer P, Rasch C, Lebesque JV. The probability of correct target dosage: dose-population histograms for deriving treatment margins in radiotherapy. *Int J Radiat Oncol Biol Phys*. 2000;47:1121-1135.

29. Wolthaus JW, Schneider C, Sonke JJ, et al. Mid-ventilation CT scan construction from four-dimensional respiration-correlated CT scans for radiotherapy planning of lung cancer patients. *Int J Radiat Oncol Biol Phys*. 2006;65:1560-1571.

30. Peulen H, Belderbos J, Rossi M, Sonke JJ. Mid-ventilation based PTV margins in Stereotactic Body Radiotherapy (SBRT): a clinical evaluation. *Radiother Oncol*. 2014;110:511-516.

31. Witte MG, van der Geer J, Schneider C, Lebesque JV, van Herk M. The effects of target size and tissue density on the minimum margin required for random errors. *Med Phys*. 2004;31:3068-3079.

32. Evaluation of measurement data—Guide to the expression of uncertainty in measurement, International Organization for Standardization (ISO), Joint Committee for Guides in Metrology (JCGM 100, 2008), corrected version 2010. Accessed April 1, 2023. http://www.bipm.org/utils/common/documents/jcgm/JCGM_100_2008_E.pdf

33. Matsuo Y, Hiraoka M, Karasawa K, et al. Multi-institutional phase II study on the safety and efficacy of dynamic tumor tracking-stereotactic body radiotherapy for lung tumor. *Radiother Oncol*. 2022;172:18-22.

34. Iizuka Y, Hiraoka M, Kokubo M, et al. Dynamic tumor-tracking stereotactic body radiotherapy with real-time monitoring of liver tumors using a gimbal-mounted linac: a multi-institutional phase II study. *Clin Transl Radiat Oncol*. 2023;39:100591.

35. Kyoto University. *Phase II Study of Dynamic Tumor Tracking Intensity-Modulated Radiotherapy in Patients with Locally Advanced Pancreatic Cancer*. UMIN; 2015. (Jan 1, 2021, date last accessed). https://upload.umin.ac.jp/cgi-open-bin/ctr_e/ctr_view.cgi?recptno=R000020308

36. Garibaldi C, Russo S, Ciardo D, et al. Geometric and dosimetric accuracy and imaging dose of the real-time tumour tracking system of a gimbal mounted linac. *Phys Med*. 2015;31:501-509.

37. Mageras GS, Kutcher GJ, Leibel SA, et al. A method of incorporating organ motion uncertainties into three-dimensional conformal treatment plans. *Int J Radiat Oncol Biol Phys*. 1996;35:333-342.

38. Killoran JH, Kooy HM, Gladstone DJ, et al. A numerical simulation of organ motion and daily setup uncertainties: implications for radiation therapy. *Int J Radiat Oncol Biol Phys*. 1997;37:213-221.

39. Herschtal A, Foroudi F, Silva L, et al. Calculating geometrical margins for hypofractionated radiotherapy. *Phys Med Biol*. 2013;58:319-333.

40. Poels K, Dhont J, Verellen D, et al. A comparison of two clinical correlation models used for real-time tumor tracking of semi-periodic motion: a focus on geometrical accuracy in lung and liver cancer patients. *Radiother Oncol*. 2015;115:419-424.